BIOCHEMISTRY
including biophysical chemistry & molecular biology
Article

*Biochemistry* **2010,** *49,* 1903–1912 1903
DOI: 10.1021/bi9020567

# New Insights into the Role of Distal Histidine Flexibility in Ligand Stabilization of Dehaloperoxidase−Hemoglobin from *Amphitrite ornata*[†]

Francesco P. Nicoletti,[‡] Matthew K. Thompson,[§] Barry D. Howes,[‡] Stefan Franzen,[§] and Giulietta Smulevich*[,‡]

[‡]*Dipartimento di Chimica, Università di Firenze, Via della Lastruccia 3, I-50019 Sesto Fiorentino (FI), Italy, and*
[§]*Department of Chemistry, North Carolina State University, 2620 Yarbrough Drive, Raleigh, North Carolina 27695*

*Received December 2, 2009; Revised Manuscript Received January 14, 2010*

ABSTRACT: The present work highlights the important role played by the distal histidine in controlling the binding of heme ligands in dehaloperoxidase (DHP) as compared to myoglobin and peroxidases. In DHP the distal histidine is highly mobile and undergoes a conformational change that places it within hydrogen-bonding distance of anionic ligands and water, where strong hydrogen bonding can occur. The detailed resonance Raman (RR) analysis at room temperature shows the presence of an equilibrium between a 5-coordinate and a 6-coordinate (aquo) high-spin form. The equilibrium shifts toward the aquo form at 12 K. These two forms are consistent with the existing X-ray structures where a closed conformation, with His55 positioned in the distal pocket and H-bonded with the distal water molecule (6-coordinate), and an open solvent-exposed conformation, with the His55 displaced from the distal pocket (5-coordinate form), are in equilibrium. Moreover, the comparison between the Raman data at 298 and 12 K and the results obtained by EPR of DHP in the presence of 4-iodophenol highlights the formation of a pure 5-coordinate high-spin form (open conformation). The data reported herein support the role of His55 in facilitating the interaction of substrate and inhibitor in the regulation of enzyme function, as previously suggested. The two conformations of His55 in equilibrium at room temperature provide a level of control that permits the distal histidine to act as both the acid−base catalyst in the peroxidase mechanism and the stabilizing amino acid for exogenous heme-coordinated ligands.

Dehaloperoxidase (DHP)[1] displays significant peroxidase activity under physiological conditions while having a globin fold (*1*). Peroxidases are typically characterized by an increased polarity of the distal cavity compared to globins. Accordingly, the postulated mechanism of hydrogen peroxide activation and heterolytic bond cleavage in peroxidases relies on the concerted role played by the conserved distal Arg and His (*2*) through direct hydrogen bonds and charge stabilization (*3*−*6*). However, unlike peroxidases, the distal cavity of DHP shows the presence of only a distal His, without an Arg (*7*−*9*). Therefore, it appears that the mechanism of hydrogen peroxide activation in DHP is controlled entirely by the distal His.

In general, heme pocket distal amino acid residues control ligand binding in heme proteins. However, while in hemoglobin and myoglobin the distal His tunes the ligand affinities via hydrogen bond stabilization involving its $N_\varepsilon$ proton (*10*), the crystal structures and the spectroscopic study of the $CN^-$, NO, CO, and $F^-$ adducts of peroxidases revealed that significant changes are induced in the distal cavity upon adduct formation, suggesting that the distal Arg and His residues are significantly perturbed (*11*, *12*). In addition, the comparison of the UV−vis and RR spectra of the fluoride and hydroxide complexes of various peroxidases and selected mutants has highlighted the complex mechanism of stabilization of anionic ligands exerted by the distal amino acids (*13*−*16*). This mechanism resembles that of compound I formation during peroxidase catalysis, where ligand stabilization by the distal arginine is coupled to protonation of the distal histidine (*12*, *17*). Both the distal Arg and His participate, in a concerted manner, in hydrogen-bonding interactions with the ligand. However, for cytochrome *c* peroxidase (CCP), it has been shown that the interaction between Arg48 and the anions is possible because the distal Arg undergoes a conformational change that places it within hydrogen-bonding distance of bound fluoride or hydrogen peroxide, which facilitates acid−base catalysis (*11*, *12*).

Since the specific interaction with Arg is missing in DHP, it is of interest to understand whether the different cavity characteristics of DHP, the globins, and peroxidases are also reflected in the binding of exogenous ligands. Therefore, we undertook a detailed spectroscopic investigation of the ferric−fluoride and hydroxide-ligated forms to highlight how the distal heme protein cavity interacts with the exogenous ligand in comparison with Mb and peroxidases.

The flexibility of the distal histidine is key for determining its ability to interact with heme-coordinated ligands. In many heme proteins, temperature, pH, and inhibitor or substrate binding in the distal pocket are all factors that regulate the conformation of the distal histidine (*18*, *19*). For native DHP, the room temperature

[†]This work was supported by the U.S. Army Research Office (Grant 52278-LS) and local Italian grants (ex60%).

*Corresponding author. Tel: +39 0554573083. Fax: +39 0554573077. E-mail: giulietta.smulevich@unifi.it.

[1]Abbreviations: DHP, dehaloperoxidase; DHP-CN, metcyano dehaloperoxidase; DHP-CO, carbonmonoxy dehaloperoxidase; CCP, cytochrome *c* peroxidase; Hb, hemoglobin; Mb, myoglobin; SWMb, sperm whale myoglobin; HHMb, horse heart myoglobin; HRP, horseradish peroxidase; DHP-F, dehaloperoxidase fluoride; DHP-OH, dehaloperoxidase hydroxide; 4CP, 4-chlorophenol; 4BP, 4-bromophenol; 4IP, 4-iodophenol; DCP, 2,4-dichlorophenol; TBP, 2,4,6-tribromophenol; TCP, 2,4,6-trichlorophenol; TFP, 2,4,6-trifluorophenol; RR, resonance Raman; EPR, electron paramagnetic resonance; 5c, 5-coordinate; 6c, 6-coordinate; HS, high-spin state.


Published on Web 01/14/2010

X-ray crystal structure showed that there are two conformations of the distal histidine at pH 6.0. Comparison with two X-ray crystal structures at 100 K suggests that these two conformations are associated with an unusual flexibility of the distal His55 (*7*−*9*). The 100 K structures consist of a closed conformation with His55 positioned in the distal pocket and H-bonded with the distal water molecule in the metaquo form (PDB 2QFK) and an open solvent-exposed conformation with the His55 displaced from the distal pocket in the 5-coordinate deoxy form (PDB 3DR9). The open form is also the only form observed when 4-iodophenol (4IP) binds in the internal binding site (*9*). The X-ray structural data suggest that His55 is stabilized in the closed conformation by hydrogen bonding to heme ligands (*7*). Unlike 4IP, no X-ray structure is available for DHP bound to a 2,4,6-trihalophenol. However, data are available in solution. In particular, 2,4,6-trifluorophenol (TFP) has been found to bind at low temperature (< 260 K) but not at room temperature by cryogenic FT-IR, EPR, and HYSCORE studies (*20*, *21*). In addition, $^{19}$F NMR and relaxation experiments suggested that 2,4,6-TFP binds externally to the heme distal cavity at ambient temperature (*22*). Moreover, recent assignment of the backbone $^{13}C\alpha$, $^{13}C\beta$, carbonyl $^{13}$C, amide $^{1}$H, and amide $^{15}$N resonances in DHP provides further evidence for the existence of distinct binding sites which allows to distinguish substrates and inhibitors. The substrates 2,4,6-TXP (X = Br, Cl, F) bind externally, and inhibitors 4-XP bind within the distal pocket. The NMR data show that shifts in the His55 position are coupled to binding of both the substrate and inhibitor. Hence, the flexibility of the distal histidine, His55, appears to have functional relevance for inhibition (*23*). The detailed spectroscopic investigation of the ferric form in the presence of different halogenated phenols undertaken in the present work further corroborates the unusual flexibility of the distal His55.

## MATERIALS AND METHODS

*Materials*. DHP was expressed in *Escherichia coli* and purified as previously described (*24*). Purification using CM52 cation-exchange cellulose (Whatman, Clifton, NJ) in a 55 mL FLEXCOLUMN (Kimble/Kontes, Vineland, NJ) allowed us to completely remove imidazole contaminant. Isotopically enriched water ($H_2{}^{18}O$) (95%) and $D_2O$ (99.8%) was purchased from Cambridge Isotope Laboratories (USA) and Merck AG (Darmstadt, Germany), respectively. The substrate analogues 4-iodophenol and 2,4,6-trifluorophenol were purchased from Acros (New Jersey). All the other chemicals were obtained from Merck AG (Darmstadt, Germany). All chemicals were of analytical or reagent grade and were used without further purification.

*Sample Preparation*. Ferric DHP samples were prepared in 150 mM potassium phosphate, pH 6.0. Completely oxidized DHP samples were prepared by oxidation of the significant amount of the oxy−ferrous form present, due to the high protein affinity for oxygen, using excess potassium hexacyanoferrate(III) followed by gel filtration on a Bio-Gel P-6DG column equilibrated with the 150 mM phosphate buffer at pH 6 to remove the oxidant. The DHP-F complex, in 150 mM potassium phosphate at pH 5.0, was prepared by adding a 0.018 M solution of NaF to the sample, giving a final concentration of 0.015 M. The samples at pH 5 were obtained by addition of citric acid to the samples at pH 6, reaching a final concentration of 110 mM. The DHP-OH sample was prepared in 150 mM potassium phosphate at pH 9.6. The hydroxyl complexes in isotopically enriched water were prepared by adding 5 $\mu$L of DHP, in 150 mM natural abundance potassium phosphate at pH 11, to 45 $\mu$L of $D_2O$ and $H_2{}^{18}O$ to obtain a final pD 10 and pH 9.6, respectively. The 4IP-DHP ($K_D$ 318 $\mu$M) sample was prepared by diluting a 200 $\mu$M, pH 6, DHP solution with a saturated 4IP solution (1 mM) in 150 mM potassium phosphate at pH 6 to yield final concentrations of 900 $\mu$M for 4IPh and 30 $\mu$M for DHP. The 4IP:DHP molar ratio of 30:1 was employed since titration of DHP with 4IP revealed progressive variations in the DHP absorption spectrum, reaching a final form for the 30:1 molar ratio (data not shown). The TFP-DHP samples were prepared by using a range from 10- to 320-fold excess of TFP with respect to DHP. The concentration of all the samples was between 15 and 200 $\mu$M. The sample concentration was determined using the molar absorptivity of 116.4 $mM^{-1}$ $cm^{-1}$ at 406 nm (*25*). All samples for low-temperature measurements were prepared in 150 mM phosphate and 30% (v/v) glycerol. It is noted that the room temperature UV−vis and RR spectra of corresponding samples in the presence and absence of glycerol were identical.

*Spectroscopy*. (*A*) *Room Temperature*. Electronic absorption spectra were measured with a double-beam Cary 5 spectrophotometer (Varian, Palo Alto, CA). The electronic absorption spectra were obtained using a 5 mm NMR tube or a 1 mm cuvette and a 600 nm/min scan rate. The RR spectra were obtained using a 5 mm NMR tube and by excitation with the 406.7 and 413.1 nm lines of a $Kr^+$ laser (Coherent, Innova 300 C, Santa Clara, CA) and the 514.5 nm line of an $Ar^+$ laser (Coherent, Innova 90/5, Santa Clara, CA). Backscattered light from a slowly rotating NMR tube was collected and focused into a triple spectrometer (consisting of two Acton Research SpectraPro 2300i and a SpectraPro 2500i in the final stage with a 3600 groove/mm grating) working in the subtractive mode, equipped with a liquid nitrogen-cooled CCD detector. It should be noted that the spectral resolution of the RR spectra cited in the figure captions is that calculated theoretically on the basis of the optical properties of the spectrometer. However, for the moderately broad experimental RR bands observed in the present study (ca. 10 $cm^{-1}$), the effective spectral resolution will in general be lower. All RR measurements were repeated several times under the same conditions to ensure reproducibility. To improve the signal/noise ratio, a number of spectra were accumulated and summed only if no spectral differences were noted. The RR spectra were calibrated with indene, $CCl_4$, and dimethyl sulfoxide as standards to an accuracy of $\pm 1$ $cm^{-1}$ for intense isolated bands. To determine peak intensities and positions a curve-fitting program (Lab Calc; Galactic) was used to simulate the spectra using a Lorentzian line shape with bandwidths between 10 and 13 $cm^{-1}$. In particular, 10 $cm^{-1}$ has been used to fit the $B_{1g}$ modes, 11 $cm^{-1}$ for the vinyl modes, 12 $cm^{-1}$ for the $E_u$ modes, and 13 $cm^{-1}$ for the $A_{1g}$ and $A_{2g}$ modes.

(*B*) *Low Temperature*. The low-temperature experiments were carried out using an Air Products Displex closed-cycle He refrigerator with automatic temperature control.

For the low-temperature RR measurements, 20 $\mu$L of the protein solution was deposited on the copper cold finger of the refrigerator at 90 K under a nitrogen flow. The temperature was then slowly decreased to 12 K under vacuum, and RR spectra were obtained at this temperature. The backscattered light was collected and focused into a computer-controlled double monochromator (Jobin-Yvon HG2S) equipped with a cooled photomultiplier (RCA C31034 A) and photon-counting electronics. The RR spectra were calibrated with indene as standard to an

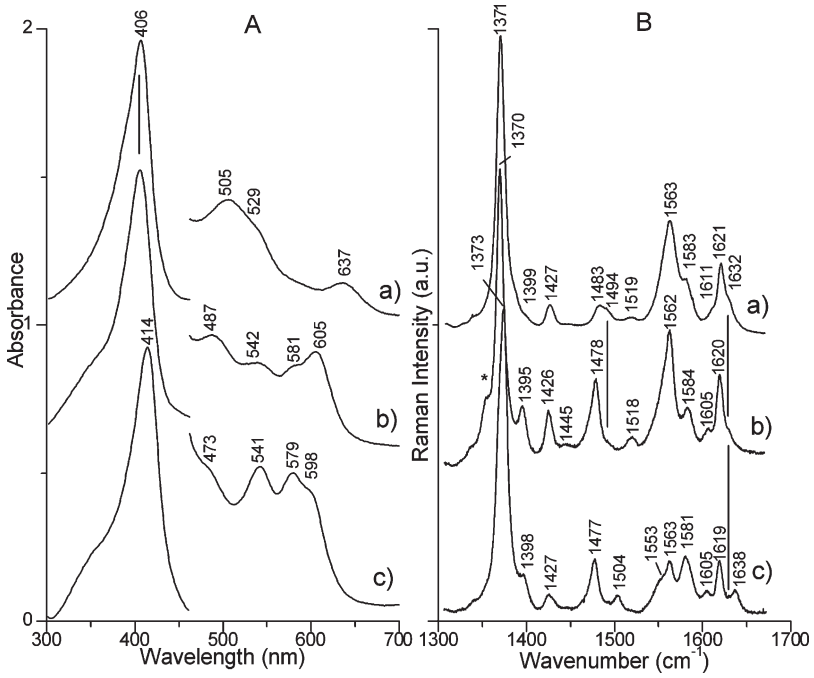


FIGURE 1: Electronic absorption spectra (panel A) and RR spectra (panel B) of ($Fe^{3+}$)DHP at pH 6 (a), ($Fe^{3+}$)DHP-F at pH 5 (b), and ($Fe^{3+}$)-DHP-OH at pH 9.6 (c) in 0.15 M potassium phosphate. The 460−700 nm region (panel A) has been expanded by a factor of 5. Experimental conditions for panel B: (a) 406.7 nm excitation wavelength, 5 mW laser power at the sample, average of 6 spectra with 300 s integration time, 1.3 $cm^{-1}$ spectral resolution; (b) 406.7 nm excitation wavelength, 5 mW laser power at the sample, average of 12 spectra with 300 s integration time, 1.3 $cm^{-1}$ spectral resolution; the asterisk indicates the reduced form (1354 $cm^{-1}$); (c) 413.1 nm excitation wavelength, 6 mW laser power at the sample, average of 3 spectra with 600 s integration time, 1.2 $cm^{-1}$ spectral resolution. The intensities are normalized to that of the $\nu_4$ band. Spectra have been shifted along the ordinate axis to allow better visualization.

accuracy of ±1 $cm^{-1}$ for intense isolated bands. The glycerol bands were subtracted from the RR spectra of the samples.

EPR spectra were recorded on a Bruker Elexys E500 instrument equipped with a microwave frequency counter. An Oxford Instruments ESR 900 cryostat was used to obtain low temperatures. The spectra were recorded under nonsaturating conditions at 5 K, 1 mW microwave power, and 1 mT modulation amplitude. The EPR simulation program used to determine the $g$ values (Xsophe; Bruker) is appropriate for effective $S = {}^1/_2$ systems.

## RESULTS

*Room Temperature*. (*A*) *Native Protein*. The absorption spectrum of metaquo DHP at pH 6.0 (Figure 1, panel A, trace a) is characterized by a Soret band at 406 nm, $Q_1$ and $Q_0$ bands at 505 and 529 nm, respectively, and the charge transfer (CT1) band (long wavelength, >600 nm porphyrin-to-metal charge transfer band) at 637 nm, very similar to the spectrum of metaquo Mb (*26*). Therefore, the spectrum, almost identical to those previously reported (*25*, *27*), is typical of a high-spin species. Accordingly, the corresponding RR spectrum (Figure 1, panel B, trace a) indicates an equilibrium between a predominant hexacoordinated high-spin species (6cHS) ($\nu_3$ at 1483 $cm^{-1}$, $\nu_2$ at 1563 $cm^{-1}$, and $\nu_{10}$ at 1611 $cm^{-1}$) and a pentacoordinated high-spin species (5cHS) ($\nu_3$ at 1494 $cm^{-1}$). These two forms are consistent with the existing X-ray structures where a closed conformation with His55 positioned in the distal pocket (6-coordinate) and an open solvent-exposed conformation with the His55 displaced from the distal pocket (5-coordinate form) are in equilibrium (Figure 2, center top) (*9*). In a previous study, RR spectra showing a mixture of a high-spin and a low-spin species were obtained (*27*), the latter due to a bis-imidazole complex resulting from the presence of an imidazole impurity (see Materials and Methods).

Unlike Mb, which is characterized by two coincident $\nu_{(C=C)}$ stretching modes at 1621 $cm^{-1}$ (*28*), on the basis of depolarization ratio measurements obtained by a curve-fitting analysis (Figure 3, panel A), two polarized bands (Table 1) are observed for DHP at 1621 and 1632 $cm^{-1}$ which are therefore assigned to two vinyl stretching modes. A direct relationship between the $\nu_{(C=C)}$ stretching wavenumber and the orientations of the vinyl groups (i.e., their torsional angles), as induced by specific protein interactions, has been established for heme-containing peroxidases and myoglobin (*29*). Therefore, this result is consistent with the crystal structure of DHP (*8*) which shows two different torsional angles of −144° and 158° for 2- and 4-vinyl, respectively.

(*B*) *Binding of Anionic Ligands*. Upon addition of fluoride to the protein at pH 5.0 marked changes are observed in the UV−vis spectrum (Figure 1, panel A, trace b). In accord with previously reported results (*27*), the spectrum of the DHP-F adduct is characterized by a Soret band maximum at 406 nm and a CT1 band at 605 nm, which is 5 nm blue shifted compared to the corresponding band of the Mb−F complex (*16*). The corresponding RR spectrum is typical of a 6cHS form (Figure 1, panel B, trace b) with $\nu_3$ at 1478 $cm^{-1}$, $\nu_2$ at 1562 $cm^{-1}$, and $\nu_{10}$ at 1605 $cm^{-1}$. A small amount of a 5cHS unligated protein ($\nu_3$ at 1494 $cm^{-1}$) is observed. As in the met form, but different from Mb, two $\nu_{(C=C)}$ vinyl stretching modes are observed at 1620 and 1632 $cm^{-1}$ (Figure 3, panel B).

The UV−vis spectrum of DHP at alkaline pH (pH 9.6) (Figure 1, panel A, trace c) is characteristic of a mixture of 6-coordinate low-spin (6cLS) (maxima at 414, 541, and 579 nm) and 6cHS (CT at 473 and 598 nm) species with a hydroxyl group

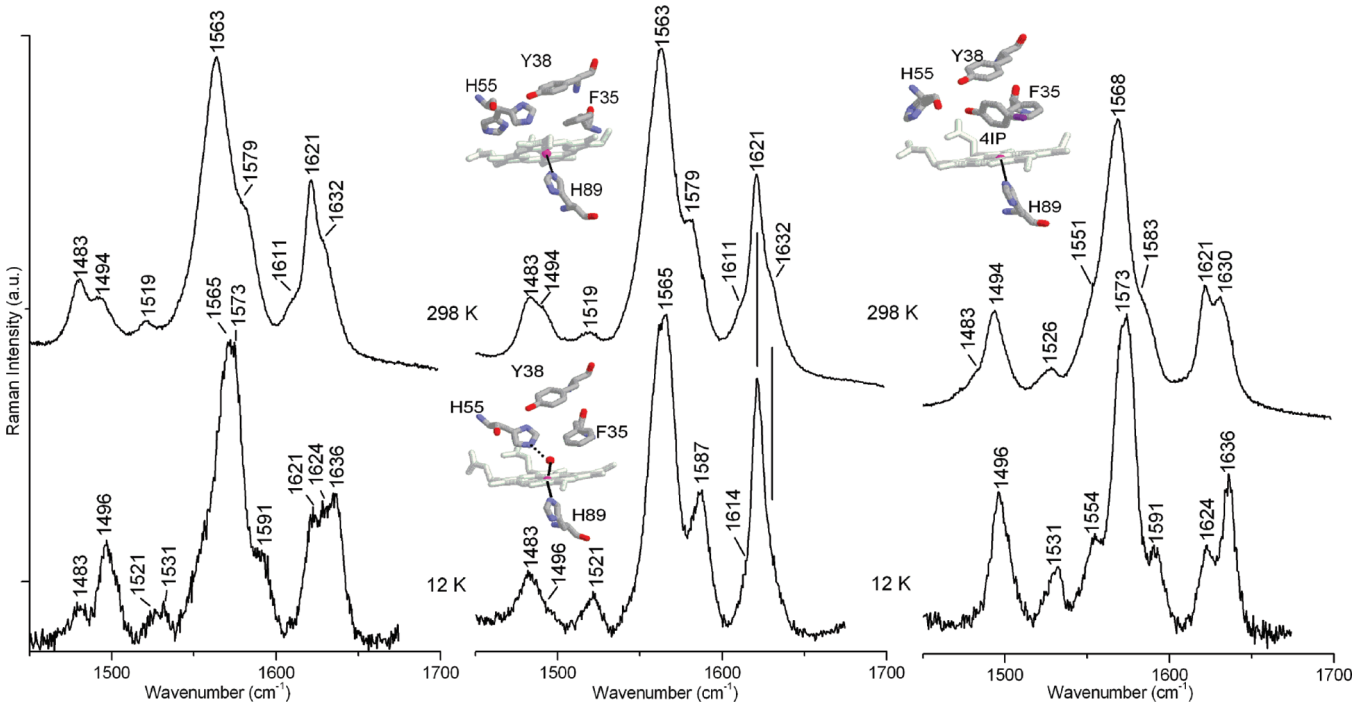


FIGURE 2: RR spectra of DHP (center), DHP-4IP (1:30 molar ratio) (right), and DHP-TFP (1:320 molar ratio) (left) at 298 K (top) and 12 K (bottom) at pH 6. Experimental conditions: $\lambda_{exc}$ 406.7 nm, spectral resolution 1.3 $cm^{-1}$ (298 K) and 5 $cm^{-1}$ (12 K), power at the sample 5 mW (298 K) and 8 mW (12 K). DHP: average of 6 spectra with 300 s integration time (298 K), collection interval 8 s/0.5 $cm^{-1}$ (12 K). 4IP: average of 6 spectra with 300 s integration time (298 K), collection interval 6 s/0.5 $cm^{-1}$ (12 K). TFP: average of 3 spectra with 300 s integration time (298 K), collection interval 6 s/0.5 $cm^{-1}$ (12 K). The intensities are normalized to that of the $\nu_4$. Spectra have been shifted along the ordinate axis to allow better visualization. The existing heme cavity X-ray structures are also reported. Center top, structure at room temperature (PDB: 1EW6) (*9*); center bottom, 100 K structure (PDB: 2QFK) (*8*); right top, room temperature structure of DHP-4IP (PDB: 1EWA) (*9*).

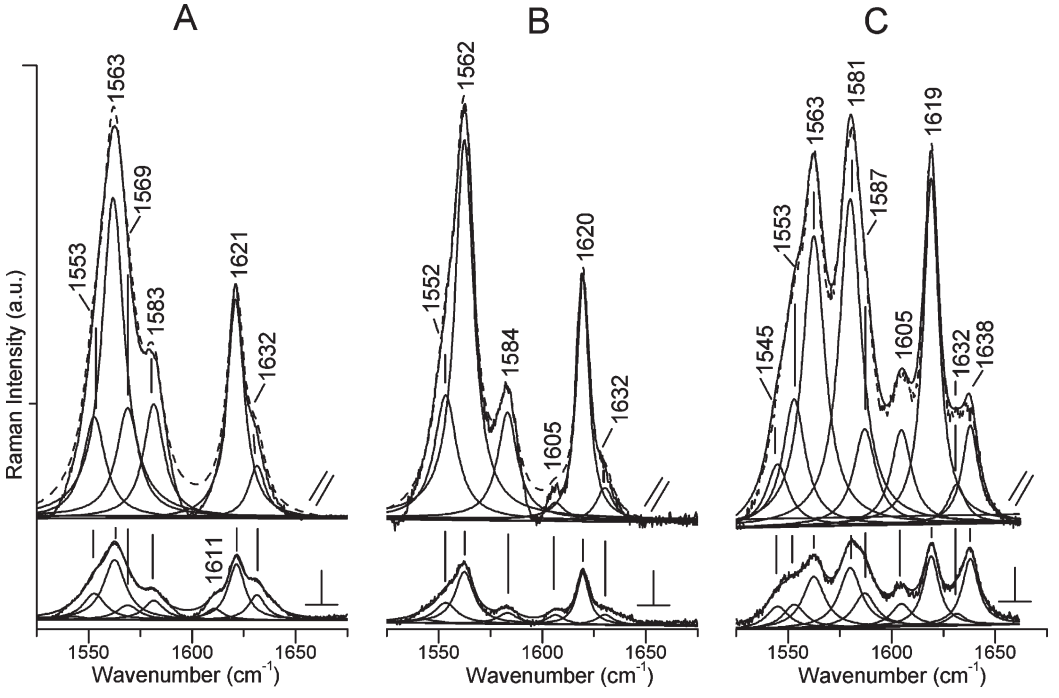


FIGURE 3: Curve fitting of the RR spectra of ($Fe^{3+}$)DHP at pH 6 (A), ($Fe^{3+}$)DHP-F at pH 5 (B), and ($Fe^{3+}$)DHP-OH at pH 9.6 (C) in 0.15 M potassium phosphate for parallel (∥) and perpendicular (⊥) polarized light, taken with 406.7 nm (A and B) and 413.1 nm (C) excitation wavelengths.

bound to the heme iron, as previously observed (*20*, *27*). This behavior is similar to that of Mb except that the Soret and the CT1 bands are 1 and 2 nm blue shifted, respectively (*13*). The corresponding RR spectrum (Figure 1, panel B, trace c) indicates the presence of a 6cLS ($\nu_3$ at 1504 $cm^{-1}$, $\nu_2$ at 1581 $cm^{-1}$, and $\nu_{10}$ at 1638 $cm^{-1}$) and a 6cHS species ($\nu_3$ at 1477 $cm^{-1}$, $\nu_2$ at 1563 $cm^{-1}$). In addition, the bands at 1619 and 1632 $cm^{-1}$ are assigned to the two $\nu_{(C=C)}$ vinyl stretches (Figure 3 panel C).

Table 1: RR Frequencies (in $cm^{-1}$) in the High Wavenumber Region of the Various Ferric DHP Species, Their Normal Mode Assignments, and Depolarization Ratios ($\rho$) (in Parentheses) Compared to Those of Mb[a]

| | | DHP | | | | | | | | Mb | | | |
|---|---|---|---|---|---|---|---|---|---|---|---|---|---|
| | | $Fe^{3+}$ | | +4IP | | $Fe^{3+}$-F | $Fe^{3+}$-OH | | | $Fe^{3+}$[g] | $Fe^{3+}F$[h] | $Fe^{3+}$-OH[i] | |
| mode | sym | 5cHS | *6cHS* | *5cHS* | 6cHS | 6cHS | *6cHS* | | 6cLS | 6cHS | 6cHS | *6cHS* | 6cLS |
| $\nu_{21}$ | $A_{2g}$ | | 1303[b] | | | | | 1304[b] | | 1307 | | | |
| $\nu_{41}$ | $E_u$ | | 1340 | | | | | 1341 | | 1341 | | | |
| $\nu_4$ | $A_{1g}$ | | 1371 (0.18) | | 1372 (0.16) | 1370 (0.15) | | 1373 (0.17) | | 1371 | 1371 | 1373 | |
| $\nu_{20}$ | $A_{2g}$ | | 1399 | | 1397 | 1395 | | 1398 | | 1401 | | | |
| $\delta(CH_2)$ | | | 1427 | | 1427 | 1426 | | 1427 | | 1426 | | | |
| $\nu_{28}$ | $B_{2g}$ | | | | | 1445 | | | | | | | |
| $\nu_3$ | $A_{1g}$ | 1494 (0.11) | 1483 (0.15) | 1494 (0.11) | 1483 (0.11) | 1478 (0.14) | 1477 (0.16) | | 1504 (0.15) | 1483 | 1482 | 1479 | 1504 |
| $\nu_{38}$ | $E_u$ | | 1519 | 1526 | | 1518 (0.21) | | | 1553 (0.22) | 1511 | | | |
| $\nu_{11}$ | $B_{1g}$ | | 1548 (0.73) | 1551 | | 1552 | 1545 | | | 1544 | 1546 | 1545 | |
| $\nu_2$ | $A_{1g}$ | | 1563 (0.18) | 1568 (0.13) | | 1562 (0.14) | 1563 (0.17) | | 1581 (0.21) | 1563 | 1556 | 1562 | 1583 |
| $\nu_{19}$ | $A_{2g}$ | 1569 (∞) | | | | | | | 1587 | | | | |
| $\nu_{37}$ | $E_u$ | | 1583 (0.22) | | 1583 (0.22) | 1584 (0.13) | | | 1605 (0.24) | 1583 | 1583 | | |
| $\nu_{(C=C)}$ | | | 1621 (0.24) | | 1622 (0.15) | 1620 (0.19) | | 1619 (0.2) | | 1621 | 1619 | 1620 | |
| $\nu_{(C=C)}$ | | | 1632[c] | | overlapped[d] | 1632 (0.33) | | 1632 (0.34) | | | | | |
| $\nu_{10}$ | $B_{1g}$ | 1632 (0.66) | 1611[c] | 1630[e] | | 1605 | | | 1638[f] | | | 1607 | 1640 |

[a]The underlined frequencies are enhanced with the 514.5 nm excitation wavelength (data not shown). The species written in italics are the most predominant. [b]Not reported in the figures. [c]$\rho$ cannot be determined due to the overlapping contribution of $\nu_{10}$ with the more intense $\nu_{(C=C)}$ band at 1621 $cm^{-1}$. [d]Overlapped with the $\nu_{10}$ at 1630 $cm^{-1}$. [e]$\rho$ (0.42) cannot be precisely determined due to the overlapping contribution between this mode and the $\nu_{(C=C)}$ at about the same frequency. [f]$\rho$ determined with 413.1 nm excitation wavelength. [g]Reference *28*. [h]Reference *30*. [i]Reference *13*.

A complete assignment of DHP, DHP-F, and DHP-OH in the high frequency region, compared to Mb, is reported in Table 1.

Figure 4 (panel A) compares the low-frequency RR spectra of WT-DHP and its adducts with fluoride and hydroxide. The DHP-F RR spectrum (Figure 4, trace b) shows a new band at 462 $cm^{-1}$, not present in the metaquo form (Figure 4, trace a). This band is assigned to the $\nu_{(Fe-F)}$ stretching mode by analogy with the corresponding band observed for Mb (*30*). The RR spectrum of DHP-OH shows new bands at 491 and 551 $cm^{-1}$ (Figure 4, trace c) which are isotope sensitive. The band at 491 downshifts to 482 $cm^{-1}$ in $D_2O$ and to 471 $cm^{-1}$ in $H_2{}^{18}O$, whereas the band at 551 $cm^{-1}$ shifts to 542 $cm^{-1}$ in $D_2O$ and to 525 $cm^{-1}$ in $H_2{}^{18}O$ (Figure 4, panel B). Therefore, they are assigned to the high-spin and low-spin Fe−OH stretching modes $\nu_{(Fe-OH)}$, respectively. Since the frequencies are identical to those previously reported for Mb (*13*), they indicate that the hydroxide derivative of DHP at room temperature exists in a thermal equilibrium between high- and low-spin states, as observed for myoglobin and other heme proteins.

The finding of two different $\nu_{(C=C)}$ vinyl stretching modes in all the ferric forms of DHP allows us to understand the slight difference observed in the electronic absorption spectra of the fluoride and hydroxyl complexes of DHP and Mb. In general, Soret and CT1 maxima shifts can occur when there are differences in the ligand field strength of the anionic ligand bound to the iron (*16*). However, the identity of the frequencies of the $\nu_{(Fe-F)}$ and $\nu_{(Fe-OH)}$ stretching modes between the two proteins allows us to exclude a different interaction between the exogenous ligand and the protein cavity. As a consequence, the blue shift of the Soret and CT1 bands between the complexes of DHP and Mb with anionic ligands derives from a different orientation of the two vinyl groups. The Soret band results from an electronic transition that involves $\pi$ and $\pi^*$ levels ($\pi \rightarrow \pi^*$), while the CT1 band is due to a transition from the $a_{2u}(\pi)$ porphyrin orbitals to $d\pi$ iron orbitals. The energy of the $\pi$ orbitals depends on the coordination/spin state of the heme and the degree of conjugation between the heme group and its two vinyl substituents. Therefore, the electronic coupling between the vinyl groups and the porphyrin modulates the $\pi \rightarrow \pi^*$ and $a_{2u}(\pi) \rightarrow d\pi$ transitions and furnishes an enhancement mechanism for the vibrational modes of the vinyl groups in the RR spectra (*31*). In most cases, the vinyl substituents give rise to polarized bands around 1620−1630 $cm^{-1}$. A lower frequency is expected to correspond to a higher degree of conjugation between the vinyl group and the porphyrin $\pi$ system. Increased conjugation with the vinyl group should shift the energy of the $\pi \rightarrow \pi^*$ and $a_{2u}(\pi) \rightarrow d\pi$ transitions to lower energy, thus shifting the Soret and CT1 maxima to the red. In Mb the two $\nu_{(C=C)}$ modes overlap at 1621 $cm^{-1}$ (*28*). On the contrary, the RR spectra of DHP clearly show the presence of two vinyl stretching modes around 1620 and 1632 $cm^{-1}$. The presence of two vinyl bands in the spectra indicates that the protein matrix imposes different constraints on the two vinyl groups (*29*). The higher $\nu_{(C=C)}$ frequency in DHP, as compared to Mb, is consistent with a lower conjugation between the vinyl group and the porphyrin $\pi$ system and, therefore, with the shift to higher energy of Soret and CT1.

The complete assignment of the high-frequency region RR modes of the WT-DHP and its complexes with small ligands and 4IP is reported in Table 1.

*Binding of Halogenated Phenols.* (*A*) *Room Temperature*. DHP has the capability to catalyze the peroxide-dependent dehalogenation of halogenated phenols (*1*). Contrasting results have been reported which suggest that substrate binding must precede $H_2O_2$ binding to optimize peroxidase activity (*24*) and vice versa (*32*). The DHP-4IP crystal structure (*9*) reveals that 4IP binds in an internal site of the distal heme cavity and forces H55 into a solvent-exposed position preventing coordination of the water molecule. Thus it is reasonable to hypothesize that the binding of this molecule affects the heme iron conformation and, therefore, its spin and coordination states. Figure 2 compares the RR spectra at pH 6 of WT-DHP (center), DHP-4IP (4IP:DHP = 30:1 molar ratio) (right), and DHP-TFP (TFP:DHP = 320:1 molar ratio) (left) complexes at room temperature (top spectra) and 12 K (bottom spectra). The existing X-ray heme cavity

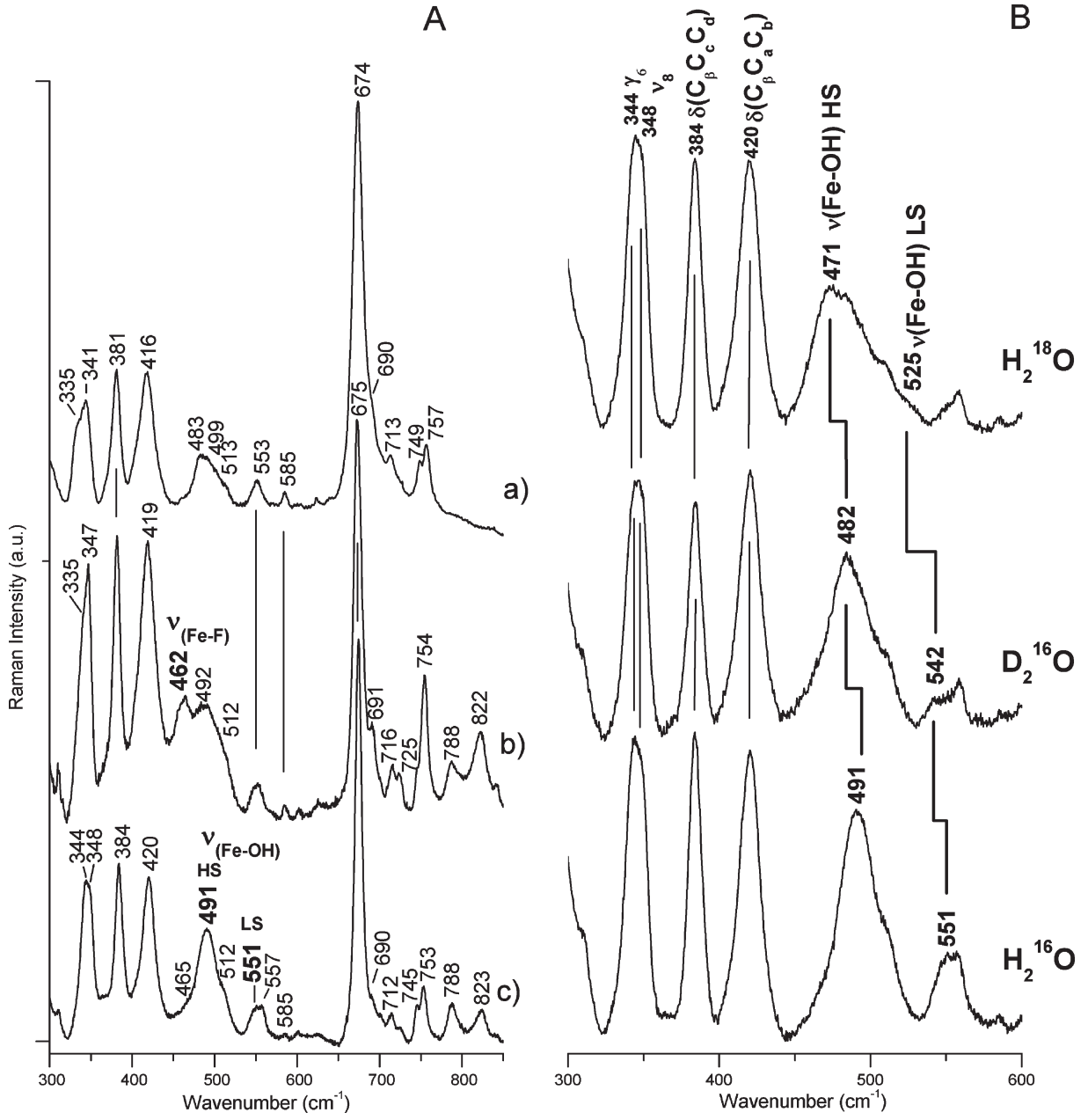


FIGURE 4: Panel A: RR spectra of ($Fe^{3+}$)DHP at pH 6 (a), ($Fe^{3+}$)DHP-F at pH 5 (b), and ($Fe^{3+}$)DHP-OH at pH 9.6 (c) in 0.15 M potassium phosphate. Experimental conditions: (a) 406.7 nm excitation wavelength, 5 mW laser power at the sample, average of 9 spectra with 300 s integration time, 1.3 $cm^{-1}$ spectral resolution; (b) 406.7 nm excitation wavelength, 5 mW laser power at the sample, average of 3 spectra with 600 s integration time, 1.3 $cm^{-1}$ spectral resolution; (c) 413.1 nm excitation wavelength, 6 mW laser power at the sample, average of 3 spectra with 900 s integration time, 1.2 $cm^{-1}$ spectral resolution. The intensities are normalized to that of the $\nu_7$. Panel B: Low-frequency region RR spectra of ($Fe^{3+}$)DHP-OH. Experimental conditions: excitation wavelength 413.1 nm, 6 mW laser power at the sample, 1.2 $cm^{-1}$ spectral resolution. $H_2O$ at pH 9.6 (average of 3 spectra with 900 s integration time), $D_2O$ at pD 10.0 (average of 12 spectra with 900 s integration time), and $H_2{}^{18}O$ at pH 9.6 (average of 18 spectra with 900 s integration time). The intensities are normalized to that of $\nu_7$ (not shown). Spectra have been shifted along the ordinate axis to allow better visualization.

structures are also shown. Upon binding 4IP, the predominant species changes from 6cHS ($\nu_3$ at 1483 $cm^{-1}$, $\nu_{37}$ at 1583 $cm^{-1}$) to 5cHS ($\nu_3$ at 1494 $cm^{-1}$, $\nu_2$ at 1568 $cm^{-1}$, $\nu_{10}$ at 1630 $cm^{-1}$). Accordingly, the broadening and 6 nm blue shift of the Soret maximum (399 nm) together with the red shift of the CT1 (641 nm) (Figure S1, Supporting Information) are consistent with the formation of a 5cHS species, as previously suggested by the room temperature crystal structure of the DHP-4IP complex (*9*) (Figure 2, right). On the basis of depolarization studies (see Table 1) the frequencies of the vinyl stretches are observed to change slightly upon 4IP binding. In particular, one mode is identified at 1622 $cm^{-1}$ while the second downshifts and overlaps with the $\nu_{10}$ mode at 1630 $cm^{-1}$. The shift in frequency of the vinyl stretching modes is in accord with the changes of the torsional angles estimated from the crystallographic data of the 4IP-DHP complex (*1*, *9*).

The binding of TFP to DHP has a quite different effect on the RR spectrum. In the presence of a 10-fold excess of TFP there are no significant differences at 298 K (and 12 K, see below) with respect to the wild-type form, while upon addition of a 40−320-fold excess of TFP at 298 K, a slight increase of 6cHS species is revealed by the intensification of the RR bands at 1483 $cm^{-1}$ ($\nu_3$) and 1611 $cm^{-1}$ ($\nu_{10}$) (Figure 2, left bottom, and Figure S2, Supporting Information).

(*B*) *Low Temperature*. The RR spectrum of WT-DHP at 12 K shows a markedly reduced amount of 5cHS, confirming the structural data obtained at 100 K by de Serrano et al. (*8*) in which the distal histidine is present only in the closed conformation (Figure 2, center bottom). These data are in agreement with the electronic absorption spectrum at 12 K, which shows a 3 nm red shift of the Soret band and 11 nm blue shift of the CT1 (data not shown). Unlike WT-DHP, the RR spectrum of the DHP-4IP complex at 12 K indicates the presence of a pure 5cHS species. The small amount of 6cHS ($\nu_3$ at 1483 $cm^{-1}$) observed at 298 K disappears, indicating a higher affinity of 4IP for DHP at low temperature. As previously noted for other heme proteins at low temperature (*13*) an increased frequency (of about 2−6 $cm^{-1}$) of the 5cHS core size marker bands is observed at low temperature in the RR spectra as a consequence of a contraction of the heme cavity. The binding of TFP to DHP has a quite different effect on the RR spectrum. In the presence of a 10-fold excess of TFP there are no significant differences at both 298 and 12 K with respect to the wild-type form; however, the RR spectrum at 12 K of the DHP-TFP complex for a 40-fold excess of TFP shows an increase of the 5cHS population ($\nu_3$ at 1496 $cm^{-1}$, $\nu_2$ at 1573 $cm^{-1}$, and $\nu_{10}$ at 1636 $cm^{-1}$) (Figure S2, Supporting Information), which becomes the only species present for a 320-fold excess (Figure 2 left top). A possible explanation of this effect is that a large excess of TFP can cause nonspecific binding of the ligand due to the packing forces exerted by the lower temperature. However, a more plausible explanation is that at room temperature the binding mechanism of TFP is different from that of 4IP. Recently $^1$H NMR, $^{19}$F NMR, and relaxation data consistent with an external binding site for TFP have been reported, but the location of that site has not been determined (*22*). The RR data at 12 K suggest that TFP binds inside the distal cavity side, as 4IP, even if binding at the external site, which might induce allosteric changes to the protein matrix forcing the distal histidine into the open conformation, cannot be completely ruled out. However, binding of TFP at the internal site at 12 K is also in agreement with cryogenic FTIR (*20*) and EPR experiments (*21*), which had shown that the substrate affects the distal pocket of DHP at cryogenic temperatures. In particular, cryogenic HYSCORE measurements showed that at a 10-fold excess of TFP relative to DHP a heme-bound water molecule in the resting state of the ferric form is displaced when the substrate binds, resulting in a transition from 6- to 5-coordinated iron (*21*).

The corresponding EPR spectra of the DHP complexes with 4IP and TFP obtained at 5 K (Figure 5) are in overall agreement with the RR spectra at 12 K. WT-DHP is characterized by a mixture of 6cHS ($g_\perp$ 6.00, $g_{||}$ 2.00) and 5cHS (6.09, 5.54, 2.00) forms (Figure 5, trace a). The progressive addition of TFP (up to 320-fold excess) leads to an increasing proportion of 5cHS with respect to 6cHS species (Figure 5, traces b and c). Addition of 4IP (30-fold excess) leads to a pure 5cHS state, characterized by a more rhombic *g* tensor (6.22, 5.50, 1.99) (Figure 5, trace d) compared to DHP alone or in the presence of TFP. The EPR bandwidth is also greater in the presence of 4IP, indicating that there is *g*-strain at these HS sites probably resulting from some structural instability which gives a distribution of values.

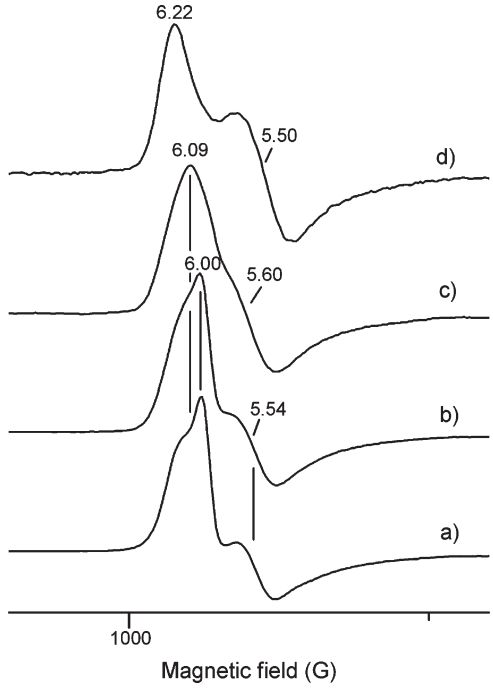


FIGURE 5: X-band EPR spectra showing the low-field $g_\perp$ region of DHP (a), DHP-TFP, 1:10 (b), and 1:320 molar ratio (c) and DHP-4IP (1:30 molar ratio) (d) at pH 6 in 0.15 M phosphate/glycerol, 30% (v/v). The spectra were recorded at 5 K, 1 mW microwave power, and 10 G modulation amplitude. Spectra have been shifted along the ordinate axis to allow better visualization.

## DISCUSSION

*Flexibility of the Distal Histidine in DHP*. (*A*) *WT-(Fe$^{3+}$)DHP*. The present spectroscopic characterization carried out in solution is in accord with the crystal structure at 298 K (*9*) in which His55 was observed to reside simultaneously in the open and closed conformations with nearly equal populations. In one of the two conformations His55 is located in the distal cavity, whereas in the second conformation it is positioned away from the distal pocket toward the solvent. The RR data clearly indicate that at room temperature the protein exists in equilibrium between the 6cHS and 5cHS states. In the 6cHS form a water molecule is coordinated to the iron and hydrogen-bonded to a distal histidine (His55), which is orientated toward the heme (closed conformation) whereas in the 5cHS state His55 is exposed to the solvent. Therefore, unlike the resting state of peroxidases, where the heme sixth coordination site is vacant or bound weakly to water (*12*), at pH 6 ferric wild-type DHP contains an metaquo 6cHS species with His55 located in the distal cavity and weakly hydrogen-bonded to the water molecule (closed conformation) (Figure 6) ($N_\delta-O_{H_2O}$ = 3.24 Å). Furthermore, at low temperature the equilibrium is shifted toward the 6cHS form (closed conformation), in perfect agreement with the recent structure obtained at 100 K which shows that, similar to the distance observed in myoglobin at neutral pH (*7*), the His55 is 0.75 Å closer to the heme iron than in the 298 K structure (*9*).

(*B*) *(Fe$^{3+}$)DHP in the Presence Halogenated Phenols*. The internal binding site of DHP has been characterized by X-ray crystallography (*9*, *33*). The structure of the DHP-4IP complex shows that the monohalophenol binding pocket is surrounded largely by hydrophobic residues (F21, F24, F35, F52, V59, F60, and L100) as well as a tyrosine (Y38). The hydroxyl group of the 4IP substrate can act as a hydrogen bond acceptor for the hydroxyl group of Y38 (distance 3.7 Å), with the distal His positioned out of the cavity (open conformation) (*9*). As a consequence, no water molecule is observed in the close vicinity of the Fe atom, and accordingly, the RR spectra are characteristic of a mainly 5cHS heme. Moreover, as observed in the X-ray structure at room temperature, the RR data confirm the changes in the

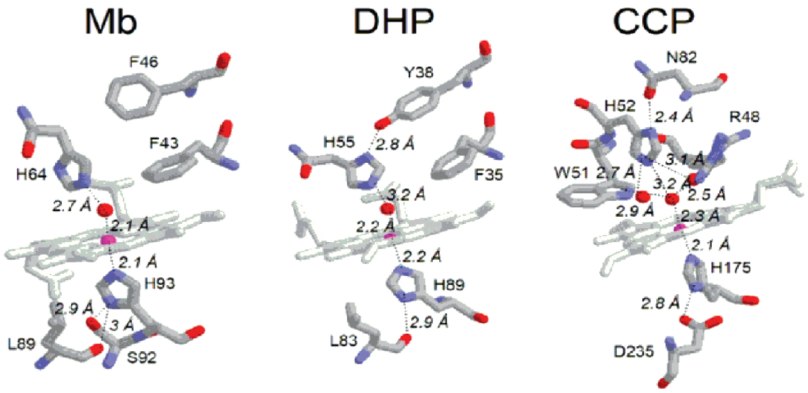


FIGURE 6: Comparison between the heme binding pockets of ($Fe^{3+}$)Mb (PDB code 1A6K) (*36*), ($Fe^{3+}$)DHP (PDB code 2QFK (subunit A)) (*8*), and ($Fe^{3+}$)CCP (PDB code 1ZBY) (*42*), showing the key residues and water molecules in each case.

vinyl orientation upon 4IP binding. At low temperature, RR core size marker bands and EPR clearly indicate that only the 5cHS species exists. Therefore, at cryogenic temperature the equilibrium of distal histidine conformations shifts toward the open conformation, indicating the stabilization of 4IP in the distal pocket binding site at low temperature. Unlike 4IP, at room temperature TFP binds in an external binding site of the heme (*22*) maintaining the 6cHS coordination of the resting protein, while at 15 K an increased amount of 5cHS is observed, leading us to conclude, in agreement with previous reports (*20*, *21*), that TFP binds inside the distal cavity, as 4IP, forcing the distal histidine in the open conformation.

*Push*−*Pull Effect in* ($Fe^{3+}$) *DHP Compared to Peroxidases and Globins*. The heme enzyme DHP is a hemoglobin known to have excellent peroxidase activity under physiological conditions (*1*, *24*). For heme-containing peroxidases, the postulated mechanism of peroxide decomposition relies on the concerted roles played by the conserved proximal histidine and the distal histidine and arginine through H-bonds and charge stabilization (*12*). However, unlike peroxidases, DHP lacks some of the main features which determine the peroxidase activity: on the distal side of the heme in peroxidases, the conserved positively charged guanidinium of an arginine residue and an H-bond from the distal histidine $N_\delta$ atom to a nearby asparagine (2.4 Å in CCP, Figure 6, right) depress the histidine p$K_a$, constraining $N_\varepsilon$ to act as a H-bond acceptor during the catalytic cycle (*34*). Although the Tyr38 residue of DHP has a strong interaction with H55 (Figure 6, middle), the p$K_a$ of H55 is approximately 4.5, which is identical to that in Mb at room temperature (*35*). Moreover, the Y38F mutant appears to have a greater initial catalytic rate than wild type. Hence, in DHP there is no obvious analogue to the arginine interaction in peroxidases.

In general, the DHP secondary structure is very similar to that of SWMb (*36*) with the overall disposition of the key α-helices (B, C, D, E, and F) nearly identical. However, on the distal side, His55 in DHP has been reported at different distances from the heme iron, ranging from 5.4 Å (*9*) to 4.8 Å (*8*). While the first reported distance is more similar to the distal cavity of peroxidases than globins, the second structure reports a distance closer to that observed in other globins including SWMb, where the distal His64 is 4.3 Å from the heme iron and H-bonded to a distal water molecule (Figure 6, left). Nevertheless, the close similarity of the frequencies of the $\nu_{(Fe-F)}$ (462 $cm^{-1}$) and $\nu_{(Fe-OH)}$ (491 and 551 $cm^{-1}$ for the HS and LS forms, respectively) stretching modes in the fluoride and hydroxyl adducts of DHP and Mb (*13*, *30*) but markedly different from the corresponding frequencies observed in peroxidases ($\nu_{(Fe-F)}$ at 385 $cm^{-1}$ for HRP (*37*) and only a LS $\nu_{(Fe-OH)}$ around 500−507 $cm^{-1}$ for various peroxidases (*13*, *38*−*40*)) clearly indicates that these ligands bind the heme iron in a similar manner in both DHP and Mb but quite different from that of peroxidases. In particular, in peroxidases, the Arg is determinant in controlling the ligand binding via a strong hydrogen bond between the positively charged guanidinium group and the anion (*13*, *15*, *16*, *41*). Recently, a high-resolution X-ray structure of resting state CCP revealed that the key residue for the formation of the catalytic intermediate compound, distal Arg48, occupies two positions: one "out" positioned close to the heme propionate and the other "in" positioned close to the heme iron. In the catalytic intermediate compound only the "in" position exists, which enables Arg48 to H-bond with the ferryl O ligand (*42*). The "in" position has been observed also in the CCP fluoride complex where the Arg48 guanidinium group moves about 2.5 Å toward the ligand to form a hydrogen bond with fluoride (*11*). Therefore, while in peroxidases the distal His contributes to the stability of the fluoride complex presumably by accepting a proton from HF and hydrogen bonding, through a water molecule, to the anion (*14*, *16*, *41*), in Mb it is the sole amino acid responsible for stabilization of the heme-coordinated ligand. The X-ray structure of the SWMb-F adduct has revealed that the fluoride anion, coordinated to the heme iron, is hydrogen-bonded to a water molecule (W195) which, in turn, is hydrogen-bonded to the $N_\varepsilon$ of the distal histidine (*10*).

On the basis of the spectroscopic results and by analogy with Mb, we suggest that a hydrogen bond network may exist between the His55, a water molecule, and the fluoride in DHP. However, this conclusion implies that the distal His, similarly to Arg48 in CCP, may undergo a conformational change that places it within hydrogen-bonding distance of the anionic ligand. In analogy to the role played by the distal Arg in CCP (*41*) the spectroscopic data suggest that the movement of the distal His55 in DHP is determinant in stabilizing only the anionic ligand binding. In fact, when other ligands without an electrical charge, such as CO and NO, are bound to the heme iron, the interaction of the distal His with the heme-bound ligand is weaker than in myoglobins. In particular, CO is an excellent probe for investigating the distal cavity of heme proteins (*43*), since back-donation from the Fe d$\pi$ to the CO $\pi^*$ orbitals is increased by polar interactions and formation of H-bonds between the bound CO and the distal protein residues. As a consequence, the Fe−C bond strengthens while the CO bond weakens, thereby increasing the $\nu_{(FeC)}$ vibrational frequencies and decreasing the $\nu_{(CO)}$ frequencies. A linear correlation with negative slope between the frequencies

of the $\nu_{(FeC)}$ and $\nu_{(CO)}$ stretching modes has been found for a large class of CO complexes of heme proteins containing imidazole as the fifth iron ligand. The $\nu_{(FeC)}/\nu_{(CO)}$ position along the correlation line reflects the type and strength of distal polar interactions. In the DHP-CO complex the slightly higher $\nu_{(CO)}$ (1950 vs 1947 $cm^{-1}$) and lower $\nu_{(FeC)}$ (499 vs 507 $cm^{-1}$) stretching frequencies than SWMb (*44*−*46*) (see Figure S3, Supporting Information) indicate a less polar environment around the CO ligand, possibly resulting from a larger distance between the CO and the imidazole. This is in agreement with the Fe−$N_{distal\ His}$ distance of 4.8−5.4 Å (*8*, *9*) vs 4.3 Å (*36*) observed in the X-ray structure of ferric DHP and Mb, respectively. In addition, recently it has been shown that the protein interactions with photolyzed NO are weaker in DHP than in the wild-type MbNO (for both SW and horse heart) (*47*).

The concerted interaction of the distal His and Arg with hydrogen peroxide bound to the heme has been called "the pull effect" (*48*−*50*). Therefore, the pull component in peroxidases is created by the distal histidine functioning as an acid/base in proton transfer to the leaving water molecule with the positively charged arginine stabilizing the developing negative charge (*48*, *50*). On the proximal side of peroxidases, the conserved H-bond between the $N_\delta$ atom of the imidazole fifth ligand and the carboxylate of an aspartic side chain, which acts as a H-bond acceptor, imparts an imidazolate character to the histidine ligand (*12*, *41*, *51*). The increased electron donation of the proximal imidazole ligand is called "the push effect" since it stabilizes the high oxidation state of the iron intermediate compound, leading to the rapid reaction of peroxidases with hydrogen peroxide (*52*).

In DHP the $N_\delta$ atom of the proximal His interacts with the carbonyl group of a Leu residue (Leu83). On the basis of the $\nu_{(Fe-Im)}$ stretching frequency of DHP (233 $cm^{-1}$), the authors concluded (*45*) that the H-bond appears to be stronger than in Mb (218−221 $cm^{-1}$) (*53*, *54*) but weaker than in peroxidases (*12*). However, a weaker imidazolate character of the proximal Fe ligand is not expected to impair the peroxidase activity of DHP (*55*). In fact, studies of proximal variants of various peroxidases clearly indicate that the "electron push" effect may not be so important for the activity since the strength of the proximal histidine−aspartate hydrogen bond can be modulated without serious effects on the peroxide cleavage step (*12*).

Therefore, the present results strongly support the view that for DHP the distal His is the only residue capable of performing proton shuttling in the active site. In the presence of negatively charged ligands, a conformational change places the distal His within hydrogen-bonding distance of the ligands, underlying its important role in anionic ligand stabilization.

## CONCLUSION

In conclusion, the present work highlights the different stabilization mechanisms of heme−iron ligands exerted by the distal residues in DHP compared to Mb and peroxidases. For the latter proteins, the Arg is determinant in controlling the ligand binding via a strong hydrogen bond between the positively charged guanidinium group and the anion. The distal His accepts a proton and is hydrogen-bonded (probably through a water molecule) with the iron-coordinated ligand. For DHP (and Mb) the distal His is the only residue responsible for the stabilization of ligands coordinated to the heme iron. However, unlike Mb, in DHP the distal His is highly mobile and undergoes a conformational change to establish a strong hydrogen bond with ligands. At room temperature, in the ferric state, in the absence of a heme ligand, the distal histidine is in equilibrium between the open solvent-exposed position (5cHS) and the closed conformation (6cHS). The equilibrium shifts to the closed conformation at 12 K. The link between the histidine and heme iron coordination extends to the binding of phenols in the distal pocket. In fact, binding of 4IP in the distal heme cavity shifts the equilibrium toward the open conformation, as the protein is in a 5cHS state, while TFP binds externally to the distal side at room temperature (6cHS) but inside the heme cavity at low temperature. When considered in the light of the recent finding that there is an external substrate binding site in DHP (*22*), the movement of H55 appears to play a role in a regulatory mechanism in DHP function. The spectra presented here show that the flexibility of the distal histidine leads to the possibility of differing hydrogen bond strength for anionic and neutral ligands to the heme iron. This level of control may, in turn, be important in explaining how a single distal histidine can provide the peroxidase "pull" that is usually thought to require the concerted action of an arginine in proximity to the distal histidine.

## ACKNOWLEDGMENT

We thank Dr. Maria Fittipaldi for provision of EPR facilities and assistance in recording the spectra.

## SUPPORTING INFORMATION AVAILABLE

UV−vis spectra of ($Fe^{3+}$)DHP and 4IP-($Fe^{3+}$)DHP at pH 6 in 0.15 M potassium phosphate, RR spectra of TFP-($Fe^{3+}$)DHP (40:1 molar ratio) at 298 and 12 K at pH 6 in 150 mM phosphate and 30% (v/v) glycerol, and a plot of the frequencies of the $\nu_{(FeC)}$ and $\nu_{(CO)}$ for DHP-CO at pH 7.0, Mb-CO at both pH 7.0 and 2.6, and Hb from *B. subtilis* at pH 7.0. This material is available free of charge via the Internet at http://pubs.acs.org.

## REFERENCES

1. Chen, Y. P., Woodin, S. A., Lincoln, D. E., and Lovell, C. R. (1996) An unusual dehalogenating peroxidase from the marine terebellid polychaete *Amphitrite ornata*. *J. Biol. Chem. 271*, 4609–4612.
2. Welinder, K. G. (1992) Superfamily of plant, fungal and bacterial peroxidases. *Curr. Opin. Struct. Biol. 2*, 388–393.
3. Poulos, T. L., and Kraut, J. (1980) The stereochemistry of peroxidase catalysis. *J. Biol. Chem. 255*, 8199–8205.
4. Sitter, A. J., Reczek, C. M., and Terner, J. (1985) Heme-linked ionization of horseradish peroxidase compound II monitored by the resonance Raman Fe(IV)═O stretching vibration. *J. Biol. Chem. 260*, 7515–7522.
5. Smith, A. T., and Veitch, N. C. (1998) Substrate binding and catalysis in heme peroxidases. *Curr. Opin. Chem. Biol. 2*, 269–278.
6. Vitello, L. B., Erman, J. E., Miller, M. A., Wang, J., and Kraut, J. (1993) Effect of arginine-48 replacement on the reaction between cytochrome *c* peroxidase and hydrogen peroxide. *Biochemistry 32*, 9807–9818.
7. Chen, Z., de Serrano, V., Betts, L., and Franzen, S. (2009) Distal histidine conformational flexibility in dehaloperoxidase from *Amphitrite ornata*. *Acta Crystallogr., Sect. D: Biol. Crystallogr. 65*, 34–40.
8. de Serrano, V., Chen, Z., Davis, M. F., and Franzen, S. (2007) X-ray crystal structural analysis of the binding site in the ferric and oxyferrous forms of the recombinant heme dehaloperoxidase cloned from *Amphitrite ornata*. *Acta Crystallogr., Sect. D: Biol. Crystallogr. 63*, 1094–1101.
9. LaCount, M. W., Zhang, E., Chen, Y. P., Han, K., Whitton, M. M., Lincoln, D. E., Woodin, S. A., and Lebioda, L. (2000) The crystal structure and amino acid sequence of dehaloperoxidase from *Amphitrite ornata* indicate common ancestry with globins. *J. Biol. Chem. 275*, 18712–18716.
10. Aime, S., Fasano, M., Paoletti, S., Cutruzzola, F., Desideri, A., Bolognesi, M., Rizzi, M., and Ascenzi, P. (1996) Structural determinants of fluoride and formate binding to hemoglobin and myoglobin: crystallographic and $^1$H-NMR relaxometric study. *Biophys. J. 70*, 482–488.

11. Edwards, S. L., and Poulos, T. L. (1990) Ligand binding and structural perturbations in cytochrome *c* peroxidase. A crystallographic study. *J. Biol. Chem. 265*, 2588–2595.
12. Smulevich, G., Feis, A., and Howes, B. D. (2005) Fifteen years of Raman spectroscopy of engineered heme containing peroxidases: what have we learned? *Acc. Chem. Res. 38*, 433–440.
13. Feis, A., Marzocchi, M. P., Paoli, M., and Smulevich, G. (1994) Spin state and axial ligand bonding in the hydroxide complexes of metmyoglobin, methemoglobin, and horseradish peroxidase at room and low temperatures. *Biochemistry 33*, 4577–4583.
14. Howes, B. D., Rodriguez-Lopez, J. N., Smith, A. T., and Smulevich, G. (1997) Mutation of distal residues of horseradish peroxidase: influence on substrate binding and cavity properties. *Biochemistry 36*, 1532–1543.
15. Neri, F., Indiani, C., Welinder, K. G., and Smulevich, G. (1998) Mutation of the distal arginine in *Coprinus cinereus* peroxidase—structural implications. *Eur. J. Biochem. 251*, 830–838.
16. Neri, F., Kok, D., Miller, M. A., and Smulevich, G. (1997) Fluoride binding in hemoproteins: the importance of the distal cavity structure. *Biochemistry 36*, 8947–8953.
17. Poulos, T. L., and Fenna, R. E. (1994) in Metal Ions in Biological Systems (Siegel, H., Ed.) pp 25−75, Marcel Dekker, New York.
18. Badyal, S. K., Metcalfe, C. L., Basran, J., Efimov, I., Moody, P. C., and Raven, E. L. (2008) Iron oxidation state modulates active site structure in a heme peroxidase. *Biochemistry 47*, 4403–4409.
19. Williams, P. A., Fulop, V., Garman, E. F., Saunders, N. F., Ferguson, S. J., and Hajdu, J. (1997) Haem-ligand switching during catalysis in crystals of a nitrogen-cycle enzyme. *Nature 389*, 406–412.
20. Nienhaus, K., Deng, P. C., Belyea, J., Franzen, S., and Nienhaus, G. U. (2006) Spectroscopic study of substrate binding to the carbomonoxy form of dehaloperoxidase from *Amphitrite ornata*. *J. Phys. Chem. 110*, 13264–13276.
21. Smirnova, T. I., Weber, R. T., Davis, M. F., and Franzen, S. (2008) Substrate binding triggers a switch in the iron coordination in dehaloperoxidase from *Amphitrite ornata*: HYSCORE experiments. *J. Am. Chem. Soc. 130*, 2128–2129.
22. Davis, M. F., Gracz, H., Vendeix, F. A., de Serrano, V., Somasundaram, A., Decatur, S. M., and Franzen, S. (2009) Different modes of binding of mono-, di-, and trihalogenated phenols to the hemoglobin dehaloperoxidase from *Amphitrite ornata*. *Biochemistry 48*, 2164–2172.
23. Davis, M. F., Bobay, B. G., and Franzen, S. (2010) Determination of separate inhibitor and substrate binding sites in the dehaloperoxidase-hemoglobin from *Amphitrite ornata*. *Biochemistry* (in press).
24. Belyea, J., Gilvey, L. B., Davis, M. F., Godek, M., Sit, T. L., Lommel, S. A., and Franzen, S. (2005) Enzyme function of the globin dehaloperoxidase from *Amphitrite ornata* is activated by substrate binding. *Biochemistry 44*, 15637–15644.
25. Osborne, R. L., Sumithran, S., Coggins, M. K., Chen, Y. P., Lincoln, D. E., and Dawson, J. H. (2006) Spectroscopic characterization of the ferric states of *Amphitrite ornata* dehaloperoxidase and Notomastus lobatus chloroperoxidase: His-ligated peroxidases with globin-like proximal and distal properties. *J. Inorg. Biochem. 100*, 1100–1108.
26. Eaton, W. A., and Hochstrasser, R. M. (1968) Single-crystal spectra of ferrimyoglobin complexes in polarized light. *J. Chem. Phys. 49*, 985–995.
27. Belyea, J., Belyea, C. M., Lappi, S., and Franzen, S. (2006) Resonance Raman study of ferric heme adducts of dehaloperoxidase from *Amphitrite ornata*. *Biochemistry 45*, 14275–14284.
28. Hu, S., Smith, K. M., and Spiro, T. G. (1996) Assignment of protoheme resonance Raman spectrum by heme labeling in myoglobin. *J. Am. Chem. Soc. 118*, 12638–12646.
29. Marzocchi, M. P., and Smulevich, G. (2003) Relationship between heme vinyl conformation and the protein matrix in peroxidases. *J. Raman Spectrosc. 34*, 725–736.
30. Desbois, A., Lutz, M., and Banerjee, R. (1979) Low-frequency vibrations in resonance Raman spectra of horse heart myoglobin. Iron-ligand and iron-nitrogen vibrational modes. *Biochemistry 18*, 1510–1518.
31. Spiro, T. G., and Li, X.-Y. (1988) in Biological Application of Raman Spectroscopy (Spiro, T. G., Ed.) Vol. *3*, pp 1−37, Wiley Interscience, New York.
32. Osborne, R. L., Coggins, M. K., Raner, G. M., Walla, M., and Dawson, J. H. (2009) The mechanism of oxidative halophenol dehalogenation by *Amphitrite ornata* dehaloperoxidase is initiated by $H_2O_2$ binding and involves two consecutive one-electron steps: role of ferryl intermediates. *Biochemistry 48*, 4231–4238.
33. de Serrano, V. S., Franzen, S., Thompson, M. K., Davis, M. F., Nicoletti, F. P., Howes, B. D., Smulevich, G. (2010) Two-site competitive inhibition in dehaloperoxidase-hemoglobin. Structures of the complexes of DHP with 4-fluoro- (3LB1), 4-chloro- (3LB2), 4-bromo- (3LB3), and 4-iodophenol (3LB4) have been deposited at the Protein Data Bank.
34. Smulevich, G., Miller, M. A., Kraut, J., and Spiro, T. G. (1991) Conformational change and histidine control of heme chemistry in cytochrome *c* peroxidase: resonance Raman evidence from Leu-52 and Gly-181 mutants of cytochrome *c* peroxidase. *Biochemistry 30*, 9546–9558.
35. Nienhaus, K., Nickel, E., Davis, M. F., Franzen, S., and Nienhaus, G. U. (2008) Determinants of substrate internalization in the distal pocket of dehaloperoxidase hemoglobin of *Amphitrite ornata*. *Biochemistry 47*, 12985–12994.
36. Vojtechovsky, J., Chu, K., Berendzen, J., Sweet, R. M., and Schlichting, I. (1999) Crystal structures of myoglobin-ligand complexes at near-atomic resolution. *Biophys. J. 77*, 2153–2174.
37. Yu, N. T. (1986) Resonance Raman studies of ligand binding. *Methods Enzymol. 130*, 350–409.
38. Nissum, M., Feis, A., and Smulevich, G. (1998) Characterization of soybean seed coat peroxidase: resonance Raman evidence for a structure-based classification of plant peroxidases. *Biospectroscopy 4*, 355–364.
39. Sitter, A. J., Shifflett, J. R., and Terner, J. (1988) Resonance Raman spectroscopic evidence for heme iron-hydroxide ligation in peroxidase alkaline forms. *J. Biol. Chem. 263*, 13032–13038.
40. Smulevich, G., Hu, S. Z., Rodgers, K. R., Goodin, D. B., Smith, K. M., and Spiro, T. G. (1996) Heme-protein interactions in cytochrome *c* peroxidase revealed by site-directed mutagenesis and resonance Raman spectra of isotopically labeled hemes. *Biospectroscopy 2*, 365–376.
41. Smulevich, G. (1998) Understanding heme cavity structure of peroxidases: comparison of electronic absorption and resonance Raman spectra with crystallographic results. *Biospectroscopy 4*, S3–S17.
42. Bonagura, C. A., Bhaskar, B., Shimizu, H., Li, H., Sundaramoorthy, M., McRee, D. E., Goodin, D. B., and Poulos, T. L. (2003) High-resolution crystal structures and spectroscopy of native and compound I cytochrome *c* peroxidase. *Biochemistry 42*, 5600–5608.
43. Spiro, T. G., and Wasbotten, I. H. (2005) CO as a vibrational probe of heme protein active sites. *J. Inorg. Biochem. 99*, 34–44.
44. Anderton, C. L., Hester, R. E., and Moore, J. N. (1997) A chemometric analysis of the resonance Raman spectra of mutant carbonmonoxy-myoglobins reveals the effects of polarity. *Biochim. Biophys. Acta 1338*, 107–120.
45. Franzen, S., Roach, M. P., Chen, Y.-P., Dyer, R. B., Woodruff, W. H., and Dawson, J. H. (1998) The unusual reactivities of *Amphitrite ornata Notomastus lobatus* chloroperoxidase do not imidazolate proximal heme iron ligand. *J. Am. Chem. Soc. 120*, 4658–4661.
46. Tsubaki, M., Srivastava, R. B., and Yu, N. T. (1982) Resonance Raman investigation of carbon monoxide bonding in (carbon monoxy)hemoglobin and -myoglobin: detection of Fe-CO stretching and Fe-C-O bending vibrations and influence of the quaternary structure change. *Biochemistry 21*, 1132–1140.
47. Franzen, S., Jasaitis, A., Belyea, J., Brewer, S. H., Casey, R., MacFarlane, A. W. t., Stanley, R. J., Vos, M. H., and Martin, J. L. (2006) Hydrophobic distal pocket affects NO-heme geminate recombination dynamics in dehaloperoxidase and H64V myoglobin. *J. Phys. Chem. B 110*, 14483–14493.
48. Dawson, J. H. (1988) Probing structure-function relations in heme-containing oxygenases and peroxidases. *Science 240*, 433–439.
49. Erman, J. E., Vitello, L. B., Miller, M. A., Shaw, A., Brown, K. A., and Kraut, J. (1993) Histidine 52 is a critical residue for rapid formation of cytochrome *c* peroxidase compound I. *Biochemistry 32*, 9798–9806.
50. Poulos, T. L. (1988) Heme enzyme crystal structures. *Adv. Inorg. Biochem. 7*, 1–36.
51. Smulevich, G., Mauro, J. M., Fishel, L. A., English, A. M., Kraut, J., and Spiro, T. G. (1988) Heme pocket interactions in cytochrome *c* peroxidase studied by site-directed mutagenesis and resonance Raman spectroscopy. *Biochemistry 27*, 5477–5485.
52. Finzel, B. C., Poulos, T. L., and Kraut, J. (1984) Crystal structure of yeast cytochrome *c* peroxidase refined at 1.7-Å resolution. *J. Biol. Chem. 259*, 13027–13036.
53. Argade, P. V., Sassaroli, M., Rousseau, D. L., Inubushi, T., Ikeda-Saito, M., and Lapidot, A. (1984) Confirmation of the assignment of the iron-histidine stretching mode in myoglobin. *J. Am. Chem. Soc. 106*, 6593–6596.
54. Teraoka, J., and Kitagawa, T. (1981) Structural implication of the heme-linked ionization of horseradish peroxidase probed by the Fe-histidine stretching Raman line. *J. Biol. Chem. 256*, 3969–3977.
55. Franzen, S. (2001) Effect of a charge relay on the vibrational frequencies of carbonmonoxy iron porphine adducts: the coupling of changes in axial ligand bond strength and porphine core size. *J. Am. Chem. Soc. 123*, 12578–12589.